Crystallization of Ge-Rich GeSbTe Alloys

Eloïse Rahier, Sijia Ran, Nicolas Ratel Ramond, Shuangying Ma, Lionel Calmels, Sabyasachi Saha, Cristian Mocuta, Daniel Benoit, Yannick Le Friec, Minh Anh Luong, et al.

▶ **To cite this version:**

Eloïse Rahier, Sijia Ran, Nicolas Ratel Ramond, Shuangying Ma, Lionel Calmels, et al.. Crystallization of Ge-Rich GeSbTe Alloys. ACS Applied Electronic Materials, 2022, 4 (6), pp.2682-2688. 10.1021/acsaelm.2c00038 . hal-03854074

HAL Id: hal-03854074
https://hal.science/hal-03854074v1

Submitted on 15 Nov 2022

HAL is a multi-disciplinary open access archive for the deposit and dissemination of scientific research documents, whether they are published or not. The documents may come from teaching and research institutions in France or abroad, or from public or private research centers.

L'archive ouverte pluridisciplinaire **HAL**, est destinée au dépôt et à la diffusion de documents scientifiques de niveau recherche, publiés ou non, émanant des établissements d'enseignement et de recherche français ou étrangers, des laboratoires publics ou privés.

Crystallization of Ge-rich GeSbTe Alloys: The Riddle is Solved.

Eloïse Rahier,[1,2] Sijia Ran,[1] Nicolas Ratel Ramond,[1] Shuangying Ma,[1] Lionel Calmels,[1] Sabyasachi Saha,[1] Cristian Mocuta,[3] Daniel Benoit,[2] Yannick Le Friec,[2] Minh Anh Luong,[1*] and Alain Claverie[1*]

[1]CEMES-CNRS and Université de Toulouse, 29 Rue Jeanne Marvig, 31055 Toulouse, France
[2]STMicroelectronics, 850 Rue Jean Monnet, 38920 Crolles, France
[3]Synchrotron SOLEIL, L'Orme des Merisiers, Saint-Aubin - BP 48, 91192 Gif-sur-Yvette Cedex, France

Corresponding authors: minh-anh.luong@cemes.fr and alain.claverie@cemes.fr

Abstract

Among the phase change materials, Ge-rich GeSbTe (GST) alloys are of considerable interest as they offer a much higher thermal stability than their congruent contenders, a desirable characteristic for embedded digital memories and neuromorphic devices. Up to now, the mechanisms by which such alloys crystallize and progressively switch from one resistivity state to the other remained unclear and very controversial. Using in situ synchrotron X-ray diffraction during isothermal annealing and advanced transmission electron microscopy techniques, we solved this riddle and unveil the mechanisms leading to the overall crystallization of such alloys. During annealing at 310°C, the initially homogeneous and amorphous material undergoes a progressive phase separation leading to the formation of Ge-rich regions of different compositions. During this decomposition, first formed GeTe embryos crystallize and trigger the heterogeneous crystallization of the Ge cubic phase. As the phase separation proceeds, these embryos dissolve and the Ge phase gradually builds up through the nucleation of small grains. Only when this Ge cubic phase is largely formed, the remaining amorphous matrix may locally reach the $Ge_2Sb_2Te_5$ composition at which it can crystallize as large grains. Our density functional theory calculations confirm that the quite exotic Pnma GeTe structure we have experimentally identified is more stable than the regular R3m structure at nanometric sizes.

Keywords: phase change materials, synchrotron X-ray diffraction, Ge-rich GST, crystallization, segregation, diffusion, nucleation dominated, decomposition

1. Introduction

Phase change materials (PCMs) are materials showing very different physical properties, notably optical and electrical, depending on their physical state, amorphous or crystalline [1–5]. The "canonical" alloy $Ge_2Sb_2Te_5$ (GST-225) allows today the development of a new generation of electronic memories called "e-PCM" (Electronic Phase Change Memories), where the information bit is coded by two very distinct resistive states, corresponding to the amorphous state (high resistivity) and the crystalline state (low resistivity) [6–10]. Beyond that, the ability to quasi-continuously tune their resistance states by applying electrical pulses makes PCMs excellent candidates for playing the role of artificial synapses in brain-inspired computers, where a network of artificial neurons is used to mimic the response of biological neurons to stimuli [11–13].

However, the low crystallization temperature of GST-225 (between 120 and 180°C) is at the origin of the low thermal stability of the different electrical states offered by the corresponding devices and is thus an obstacle to many possible applications, especially in the field of embedded technologies where operating temperatures are well above 200°C. To improve performances and offer stable characteristics at higher temperatures, at least for digital devices, the enrichment of canonical GST-225 with Germanium (Ge-rich GST or GGST) is one of the solutions promoted by the industry [10,14–18]. Indeed, GGST has a much higher crystallization temperature (>300°C), which guarantees the integrity of the encoded information at high temperature

Still, one key and limiting characteristic of PCMs is the thermal stability of the amorphous phase, which is associated with the high resistivity state of the devices. While being fundamental to device operation and understanding, the mechanisms by which such alloys crystallize and switch from one state to the other are still controversial. When this class of material was introduced [19,20], it was thought that the different properties of GGST were resulting from a single but unknown “golden”, Ge-rich, crystalline phase. Following this initial belief, recent theoretical papers have investigated the relative stability of different crystalline GST phases, in an attempt to find possible decomposition paths from “very Ge-rich” to “less Ge-rich” GGST alloys during annealing [21–23]. However, one may question the existence of many of the considered alloys (e.g., $Ge_{18}Sb_2Te_5$, $Ge_5Sb_2Te_3$, $Ge_3Sb_2Te_3$ or $Ge_2Sb_2Te_1$), as there is no experimental evidence that GST crystalline phases can accommodate Ge concentrations larger than that of Te in a single unit cell. In fact, the existence of such exotic Ge-rich GST alloys is usually incorrectly claimed from the chemical analysis of relatively large regions, by Energy-dispersive X-ray spectroscopy (EDX) or Electron energy loss spectroscopy (EELS), where the composition of different small, chemically different, grains can be averaged along the thickness of the sample. Alternatively, there are experimental evidences that the overall crystallization of such Ge-rich amorphous layers results in the formation of a two-phase material, where both the pure Ge and GST-225 crystalline phases coexist [14,24–27]. Still, the details of this crystallization process remain unclear, as well as the evolutions of the microstructure and local composition of the GGST layer, which are responsible for the observed resistivity changes. A clear understanding of these two characteristics of the GGST material is however required, if we want to be able to finely tune the resistivity of the PCM device by continuously switching the GGST material in intermediate resistivity states, as needed for advanced and neuromorphic applications.

For some authors Ge crystallizes first [24,27] while for the others crystallisation starts with the formation of GST grains[28]. Moreover, the observation of the crystallization of the Ge cubic phase at temperatures as low as 310-330°C, well below the temperature at which the homogeneous crystallisation of Ge is known to occur (400°C), is puzzling. Actually, this controversy and the lack of understanding of the details of the crystallization scenario result from the difficulty to infer the mechanisms leading to the overall crystallization of GGST layers from the sole characterization of samples ex situ annealed at different temperatures and durations. Clearly, a detailed characterization of the mechanisms at work during isothermal annealing and of their relative kinetics is missing.

In this work, we report the results of our investigations of the crystallization of Ge-rich GST alloys using isothermal annealing during in situ X-ray diffraction (XRD) performed at SOLEIL synchrotron (France). These results are complemented by transmission electron microscopy (TEM) observations. We show that, prior to crystallization, the initially homogeneous material undergoes phase separation in the amorphous phase. After some incubation time, a transient GeTe phase appears which triggers the heterogeneous nucleation of nanocrystals of the Ge cubic phase. Then, this Ge crystalline phase grows through the addition of new small grains while the Ge content in the remaining amorphous GST matrix concomitantly decreases until regions finally matching the GST-225 stoichiometry are generated and spontaneously crystallize. The transient phase responsible for the observed low temperature crystallization of Ge is formally identified as the Pnma phase of GeTe. Density functional theory (DFT) calculations attest that this phase is more stable than the common R3m phase for very small size crystals. These results unveil the intriguing characteristics of the three-step crystallization of Ge-rich alloys and close a long lasting controversy concerning the order and the scenario of crystallization in these alloys.

2. Samples and experimental methods

Samples used in this study consisted in 100 nm-thick GGST layers deposited by physical vapor deposition (PVD) using only one target of the same GGST composition onto naturally oxidized Si(100) wafers and covered by a 20 nm thick TiN cap layer using industrial tools. In these samples the Ge concentration is such that after phase separation and crystallization, the Ge and GST-225 phases weight each about 50% of the total volume. Diffraction experiments have been performed in situ and under N_2 gas flow, using an Anton Paar DHS 1100 furnace available on the Diffabs beamline at the synchrotron SOLEIL. The X-ray energy was monochromatized to 10975 eV using a Si(111) double crystal monochromator ($\Delta E/E \sim 10^{-4}$). The photon beam was focussed vertically (using Rh-coated mirrors) and horizontally (sagittal bended second crystal of the monochromator) into a spot of ~ 250 × 250 μm^2 (full width at half maximum, FWHM). The incidence angle of the X-ray beam on the specimen was adjusted to 10°, corresponding to the value at which the diffracted signal was optimized and free from artefacts. The diffracted signals were acquired through the acquisition of two CirPAD detector frames at two different angular positions, in order to fill the gap between detector modules [29]. One single XRD profile was acquired every 30 seconds. Quantitative information was extracted from the XRD profiles by Rietveld refinement. Scanning transmission electron microscopy (STEM) using high angle annular dark field imaging (HAADF) was used to check material inhomogeneity through Z-contrast imaging in a probe corrected JEOL JEM ARM 200F. As our previous ex situ XRD studies have shown that the incubation time, i.e. the time after which the onset of crystallization is observed, is of about several tens of minutes at 330°C[27], we have explored the 310-330°C temperature range in detail, in an effort to slow down and decompose the different mechanisms which intervene in the crystallization process.

3. Results and determination of the crystallization scenario

Figure 1 is a map showing the time-evolution of the XRD profiles during in situ annealing of the GGST specimen at 310°C. During the first 7 hours, the GGST layer stays in the amorphous phase as evidenced by the featureless shape of the diffused profile. After 9 hours, two main phases are present which are easily identified as the Ge cubic and GST-225 cubic phases, as previously observed after annealing at higher temperatures [14,24–27].

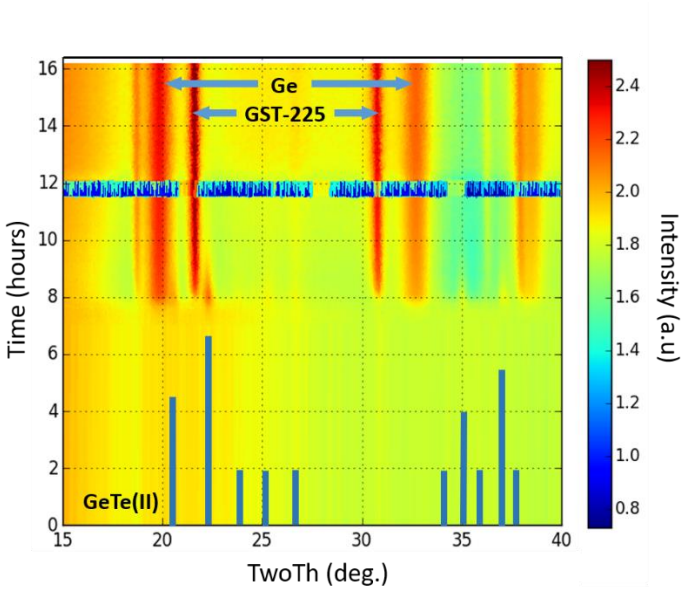

Fig. 1: XRD map obtained during in situ isothermal annealing at 310°C of an amorphous GGST layer in the synchrotron (E=10975 eV). The Ge cubic phase appears after an incubation time of nearly 7 hours, followed by the GST-225 cubic phase several minutes later. A transient phase is observed to nucleate first, just before the onset of Ge crystallization. The vertical lines show the structure factors of the GeTe Pnma structure (PDF card 00-044-0819). The blue horizontal between 41000 and 43000 seconds is due to a momentary beam loss in the synchrotron ring.

Since we are looking for the chain of events leading to the crystallization of these phases, the evolution of the diffraction profiles during this lap time is of interest. Figure 2 shows the variations of the integrated intensities of the two main characteristic peaks of the Ge and GST-225 phases during isothermal annealing.

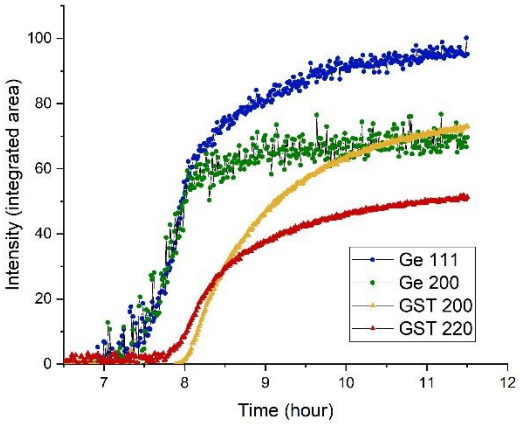

Fig. 2: Variations of the integrated diffracted intensities of the two main peaks characteristic of the Ge and GST-225 cubic phases during annealing. The GST peaks rise about 20-30 minutes after the Ge peaks have almost reached their maximum values.

This result evidences that the Ge peaks do appear before those characteristics of the GST-225 phase. The diffracted intensity of the Ge peaks dramatically increases during the first 30 minutes reaching about 70-80 % of the final values before the GST phase starts to nucleate. This is the first clear experimental evidence that GGST alloys crystallize by first nucleating the Ge phase and that the GST-225 phase crystallizes only after a large proportion of the Ge phase has already crystallized. Moreover, it should be noted that, in comparison to Ge, the GST-225 phase builds up progressively, more slowly, needing up to 90 min to diffract with an intensity of about 70 % of the final values.

Figure 3 shows the time-evolution of the mean size of the Ge and GST-225 crystallites during annealing, as extracted from the widths of the diffraction peaks and after Rietveld refinement. This figure shows that the size of the Ge crystallites remains quite constant over time, with small variations between 4 and 6 nm. Combining this information with the dramatic intensity variations observed in Figure 2, we can deduce that the crystallization of the Ge phase is nucleation-dominated, i.e. proceeds through the accumulation of new small crystallites all of about the same size. The small size increase noted from 9 to 11 hours of annealing probably results from a limited growth of existing crystals at the end of the phase separation process.

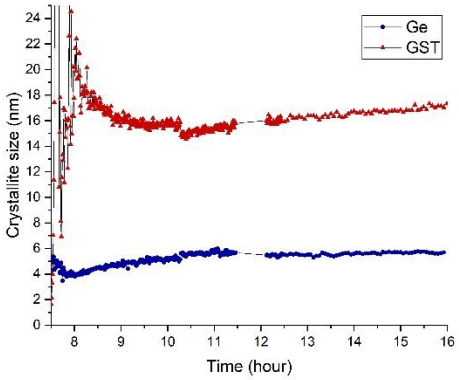

Fig. 3: Variations of the Ge and GST crystallite size during annealing. The GST grains are about 3 times larger than the Ge grains.

While nucleated later, the GST crystallites are relatively much bigger, even at the onset of crystallization, in the 15-18 nm range. They do not evolve too much during annealing. At first, they tend to decrease in size during the "nucleation period" lasting 90-120 minutes and during which the corresponding diffracted intensities increase (Fig. 2). Then, they increase again for longer annealing time, probably as a result the slight growth of the existing grains, again at the end of the phase separation process. It is important to note that these sizes are surprisingly large and well above any reported crystallite sizes observed during the nucleation-limited crystallization of pure GST-225 [30,31].

To set up and validate a scenario able to explain all the observed characteristics of the crystallization of GGST alloys, several questions must be answered. First of all, why is Ge crystallization observed as such a low temperature? The homogeneous crystallization of pure amorphous Ge is usually observed above 400°C whilst there are reports showing this mechanism can be activated at temperatures down to 380°C [32]. However, heterogeneous crystallization of Ge may occur at much lower temperatures. As an extremely favourable case, the solid phase epitaxy (SPE) of Ge, i.e. the crystallization of amorphous Ge in contact with a Ge crystalline (001) surface, can be activated at temperatures down to 310°C, still using a reasonable timescale [33].

Coming back to Figure 1 and focussing on the onset of crystallization, one can note that there are a number of distinct features in the XRD profiles which appear slightly before the appearance of the peaks corresponding to the Ge phase. In particular, a peak is clearly visible on the right side of the GST peak, at about 22°. Another weaker one is seen as a shoulder of the Ge peak, at about 20°. This evidences that a transient phase, which nucleates first then quickly disappears, is at the origin of the heterogeneous nucleation of Ge at low temperature. The quite strong peak observed at about 22° has been recently detected by Navarro's group after ex-situ annealing in the 350°C range, as a shoulder on the right side of the (200) GT-225 peak [28]. However, due to the lack of complementary peaks, the authors could not formally identify the phase responsible for this feature. Instead, they proposed that a "G$^+$GST" unknown phase forms and initiates the crystallisation of the GST-225 phase. The sensitivity of the synchrotron XRD allied to the acquisition of profiles all along the in-situ isothermal annealing

allows us to clarify this point. The broadening of the diffraction peaks corresponding to the GeTe phase is similar to that of the Ge phase. From this qualitative observation, we can infer that GeTe particles sizes are in the range of few nms. Figure 4 shows the XRD profile obtained after 30 000 s annealing i.e., during the short period when all the three phases are present. Beyond the peak at 22°, six additional peaks could be evidenced, rendering phase identification unambiguous. The transient phase, the first phase to appear at the onset of crystallisation, is identified as the dense GeTe phase (PDF card 00-044-0819), sometimes referred as type II GeTe, of orthorhombic structure (space group Pnma), and known to be the stable bulk phase under high pressure conditions [34].

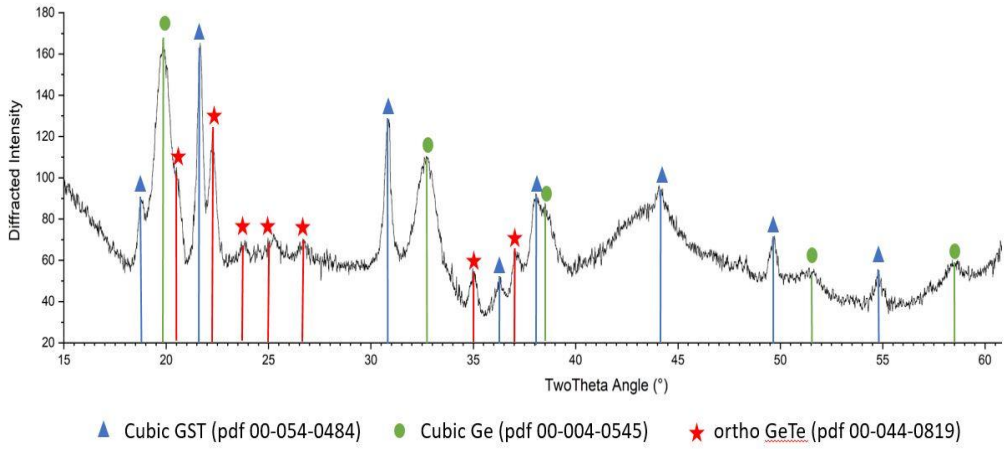

Fig. 4: XRD profile recorded after 30 000 s annealing at 310°C. The three phases are observed. The GeTe Pnma phase is formally identified through its seven characteristic peaks.

While the exhaustive study of the relative stability of facetted nanocrystals goes far beyond the scope of this paper, our DFT calculations show that not only pressure but size and termination may stabilize the orthorhombic Pnma structure at the expense of the rhombohedric R3m structure. Indeed, we have calculated the ground state energy of several slabs of the R3m and Pnma GeTe phases (with the densities of 49.75 and 52.94 Å^3/formula unit (f.u.) respectively computed for the bulk phases), terminated by different surfaces and as function of the slab thickness. For that, we have used the first-principles software VASP [35] (exchange-correlation functional PBE0sol [36], cut-off energy of 500 eV, k-mesh corresponding to $\delta k_x = \delta k_y = 0.188$ Å^{-1}, ground state energy convergence below 10^{-5} eV/f.u., force convergence of 10^{-3} eV Å^{-1}, GeTe surfaces of periodically repeated slabs separated by 20 Å of vacuum). For each of the GeTe phases and crystal orientations that we considered, we found that the ground state energy E_{slab} depends linearly on the slab thickness. This dependence can be modelled by the simple equation $E_{slab} = 2E_{surf} + nE_{bulk}$, where E_{surf} and E_{bulk} are the surface and bulk energy, respectively per GeTe surface and bulk formula unit and n is the number of GeTe atomic layers stacked in the slab.

Figure 5 shows the energy differences between R3m and Pnma GeTe stacks terminated by different surfaces, as a function of the number of GeTe atomic layers stacked in the slabs. This figure suggests that the (001) terminated Pnma phase can be more stable than the R3m phase when less than 10 GeTe layers are involved, i.e. for crystallites thinner than 3 nm. This is due to the lower energy of the GeTe (001) Pnma surfaces, the presence of which counterbalances the lowest energy of the bulk R3m phase. To check whether a modification of the inter-bilayer bonds of the slabs also contribute to the results shown in Fig. 5 beside the contribution of the surface energy [37], we have studied the variations of the inter-bilayer spacing for all the slabs considered in this figure. Noticeable variations of the inter-bilayer distance only occur in the vicinity of the first 3-4 layers the closest from the surfaces, which means that mainly surface effects (including atomic layer relaxation near the surface) contribute to the energy difference shown in Figure 5. We thus believe that the lower energy of the Pnma phase is the driving

force for the stabilization of thin nanocrystals of this phase; of course, a more rigorous calculation would have required to compute the interface energy between thin GeTe slabs and an amorphous phase of the Ge-rich GST alloys, instead of the free surfaces that we considered here.

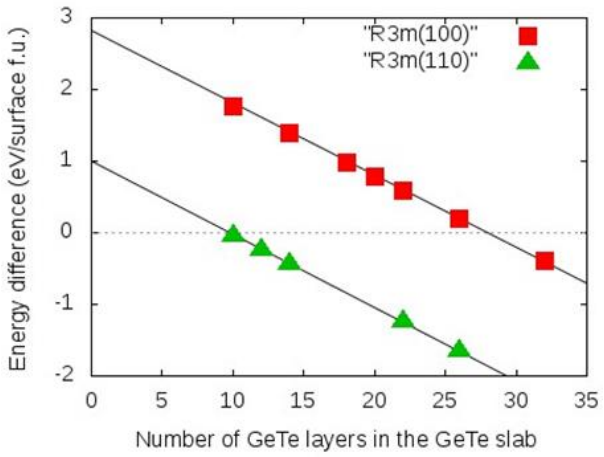

Fig. 5: Energy difference $E_{slab} - E_{slab}\{Pnma, (001)\}$, versus the number of GeTe atomic layers in the GeTe slabs. For thicknesses smaller than 10 GeTe layers, the Pnma phase is the most stable. Dark lines are guides to the eyes.

Finally, the scenario suggested by the evolution of the XRD profiles must be completed by information on the state of the material during the "incubation time" which lasts for more than 7 hours before the onset of crystallisation occurs. Figure 6 compares STEM-HAADF images of the material after deposition and after 4 hours annealing at 310°C. While the image of the as-deposited material is uniform in contrast, the annealed layer shows contrast inhomogeneity which can be ascribed to the decomposition of the layer into Ge-rich and Ge poor-regions. In other words, the material is undergoing progressive phase separation during this lap time, the matrix tempting to expulse Ge and forcing it to segregate. Interestingly, the Ge-rich regions have a diameter of a few nanometers.

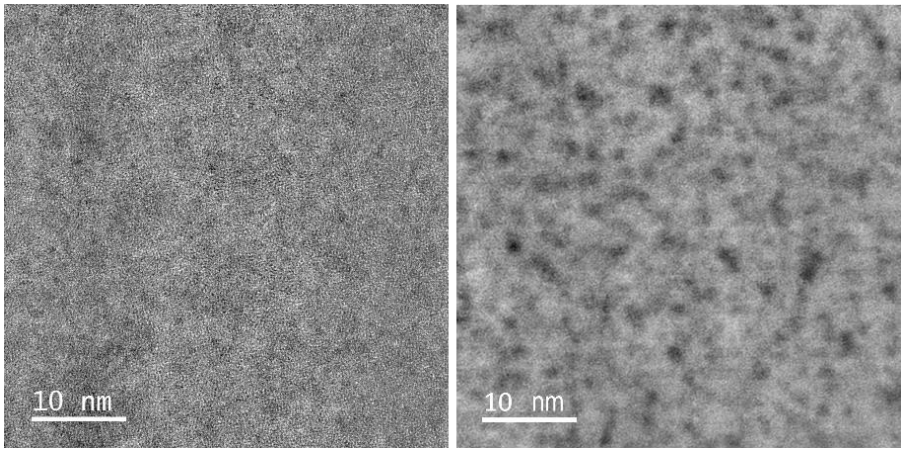

Fig. 6: STEM-HAADF images of the material, as deposited (left) and after 4 hours at 310°C (right). The dark regions seen on the image of the annealed sample are of lower "mean Z", probably due to their enrichment in Ge. These contrasts are not seen before annealing.

Putting all these results together, a scenario able to describe all the characteristics of the crystallisation of GGST alloys can now be proposed. It is illustrated in figure 7.

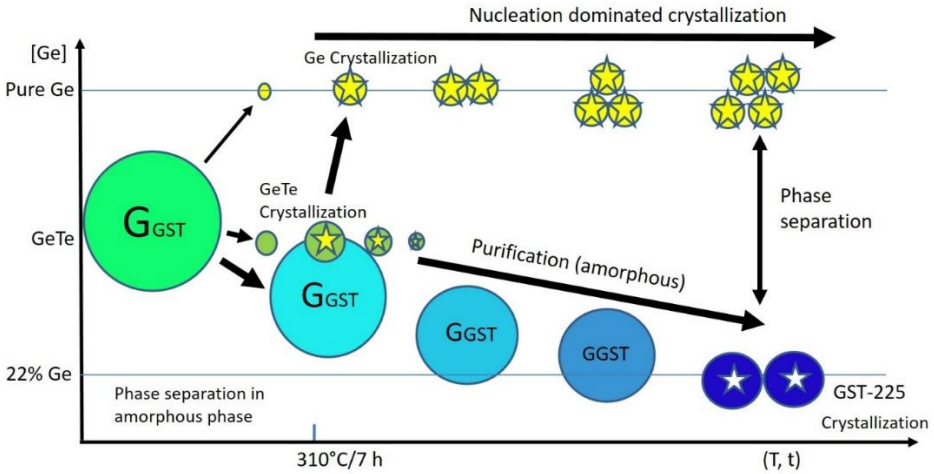

Fig. 7: Evolution of the GGST during thermal annealing. On the abscissa, the thermal energy given to the GGST material; on the ordinate, the phase composition. Circles without/with a star respectively indicate amorphous/crystalline phases. During phase separation, regions of GeTe and Ge stoichiometries are generated. In parallel, the amorphous matrix gets depleted in Ge. The crystallization of GeTe is observed after 7 hours at 310°C and triggers that of Ge through heterogeneous nucleation. The crystallization of GST-225 is observed at the end of the phase separation, when the amorphous matrix goes down to the required GST-225 stoichiometry.

This diagram shows the evolution of the system during thermal annealing and leading to the crystallization of a GGST alloy. In the amorphous state, the material is relatively homogeneous in composition but in a metastable state. As soon as sufficient thermal energy is supplied, the system decomposes by expelling and segregating the Ge and depleting the rest of the matrix. Compositional fluctuations then appear at the nanometric scale. The kinetics of the phenomenon is only limited by the capacity of the atomic Ge to diffuse in the surrounding matrix, amorphous and still rich in Ge.

As the phase separation intensifies during the incubation time, the compositional fluctuations and the low solubility of Sb in Ge [38,39] allow the formation of increasingly Ge-rich regions, until they approach the GeTe stoichiometry. As this separation is activated above 300°C, i.e. above the crystallization temperature of GeTe (around 230°C), thin GeTe grains can crystallize with the Pnma phase as soon as they are formed. Upon contact with areas richer in Ge, these GeTe crystallites trigger the heterogeneous crystallization of Ge from 310°C onwards. During annealing, the Ge phase develops, via the nucleation of new small grains and, as a consequence, the GGST matrix becomes "purified", being progressively depleted in Ge, while remaining in the amorphous phase. When the Ge content is such that the stoichiometry is locally close to that of GST-225, these regions spontaneously crystallize in the cubic GST-225 phase since the annealing temperature is much higher than the crystallization temperature of this phase (120-180°C).

This scenario well explains why GST-225 crystals appear later and are larger than observed during the crystallization of pure GST-225 [30,31]. In a GGST alloy, the crystallization of GST-225 is obtained only when very depleted Ge regions appear, i.e. when the phase separation is well advanced, which is finally obtained within larger domains. Thus, the crystallization of the GST-225 phase does not solely depend on temperature but also on a diffusion length L, i.e. on a characteristic time that depends on the temperature ($L=\sqrt{Dt}$ with $D=D_0 \exp(-E/kT)$), this is the time that the excess Ge needs to reach the (crystalline or not) Ge phase.

Finally, our findings suggest that the change of resistivity of a GGST cell submitted to some thermal processing should probably not be solely ascribed to the reduction of the size of the amorphous GGST

region in the device, but to the progressive decomposition of the GGST layer into two phases, leading to the possibility of charge carrier percolation through this composite material.

4. Conclusions

In summary, our XRD and TEM results unambiguously show that the crystallization of GGST involves its decomposition/separation into "pure" phases that crystallize successively through three steps, GeTe (fugitive), cubic Ge and finally cubic GST-225. This phase separation can be thermally activated above 310°C. The crystallization of GeTe is homogeneous and results from compositional fluctuations generated by the separation of Sb and Ge (non-miscible). These crystal seeds allow the heterogeneous crystallization of Ge at low temperature (from 310°C). The growth of the Ge phase, through the generation of small grains with a diameter of about 3-5 nm, allows the dissolution of the GeTe grains and the purification of the surviving amorphous matrix until its stoichiometry goes down to that of GST-225 where it can crystallize as large regions (> 15 nm). These phenomena are limited by the diffusion of Ge within the amorphous GGST matrix during its depletion in Ge.

Declaration of Competing Interest

The authors declare that they have no known competing financial interests.

Acknowledgements:

This work is part of the "Ô-GST Project" and partially funded by the nano2022 (IPCEI) initiative. It was granted access to the HPC resources of CALMIP supercomputing center under allocation 2020/2021-[P17025]. The authors acknowledge the synchrotron SOLEIL for allocating the beam time, and more particularly the support group of Diffabs beamline for keeping the beamline up and running.

Authors ORCID:

Sijia Ran	0000-0002-4632-0216
Nicolas Ratel-Ramond	0000-0003-4979-211X
Saha Sabyasachi	0000-0001-8051-1852
Lionel Calmels	0000-0002-0532-0404
Cristian Mocuta	0000-0001-5540-449X
Minh Anh Luong	0000-0002-0876-2400
Alain Claverie	0000-0003-2211-4618

References

(1) Wuttig, M.; Yamada, N. Phase-Change Materials for Rewriteable Data Storage. *Nature Mater* **2007**, *6* (11), 824–832. https://doi.org/10.1038/nmat2009.

(2) Lee, B. C.; Zhou, P.; Yang, J.; Zhang, Y.; Zhao, B.; Ipek, E.; Mutlu, O.; Burger, D. Phase-Change Technology and the Future of Main Memory. *IEEE Micro* **2010**, *30* (1), 143–143. https://doi.org/10.1109/MM.2010.24.

(3) Raoux, S.; Wełnic, W.; Ielmini, D. Phase Change Materials and Their Application to Nonvolatile Memories. *Chem. Rev.* **2010**, *110* (1), 240–267. https://doi.org/10.1021/cr900040x.

(4) Noé, P.; Vallée, C.; Hippert, F.; Fillot, F.; Raty, J.-Y. Phase-Change Materials for Non-Volatile Memory Devices: From Technological Challenges to Materials Science Issues. *Semicond. Sci. Technol.* **2018**, *33* (1), 013002. https://doi.org/10.1088/1361-6641/aa7c25.

(5) Guo, P.; Sarangan, A.; Agha, I. A Review of Germanium-Antimony-Telluride Phase Change Materials for Non-Volatile Memories and Optical Modulators. *Applied Sciences* **2019**, *9* (3), 530. https://doi.org/10.3390/app9030530.

(6) Bruns, G.; Merkelbach, P.; Schlockermann, C.; Salinga, M.; Wuttig, M.; Happ, T. D.; Philipp, J. B.; Kund, M. Nanosecond Switching in GeTe Phase Change Memory Cells. *Appl. Phys. Lett.* **2009**, *95* (4), 043108. https://doi.org/10.1063/1.3191670.

(7) Loke, D.; Lee, T. H.; Wang, W. J.; Shi, L. P.; Zhao, R.; Yeo, Y. C.; Chong, T. C.; Elliott, S. R. Breaking the Speed Limits of Phase-Change Memory. *Science* **2012**, *336* (6088), 1566–1569. https://doi.org/10.1126/science.1221561.

(8) Lai, S. Current status of the phase change memory and its future. Intel Corporation, RN2-05 2200 Mission College Blvd, Santa Clara, CA 95052-81 19. http://citeseerx.ist.psu.edu/viewdoc/summary?doi=10.1.1.159.9484 (accessed 2022 -04 -04).

(9) Arnaud, F.; Zuliani, P.; Reynard, J. P.; Gandolfo, A.; Disegni, F.; Mattavelli, P.; Gomiero, E.; Samanni, G.; Jahan, C.; Berthelon, R.; Weber, O.; Richard, E.; Barral, V.; Villaret, A.; Kohler, S.; Grenier, J. C.; Ranica, R.; Gallon, C.; Souhaite, A.; Ristoiu, D.; Favennec, L.; Caubet, V.; Delmedico, S.; Cherault, N.; Beneyton, R.; Chouteau, S.; Sassoulas, P. O.; Vernhet, A.; Le Friec, Y.; Domengie, F.; Scotti, L.; Pacelli, D.; Ogier, J. L.; Boucard, F.; Lagrasta, S.; Benoit, D.; Clement, L.; Boivin, P.; Ferreira, P.; Annunziata, R.; Cappelletti, P. Truly Innovative 28nm FDSOI Technology for Automotive Micro-Controller Applications Embedding 16MB Phase Change Memory. In *2018 IEEE International Electron Devices Meeting (IEDM)*; IEEE: San Francisco, CA, 2018; p 18.4.1-18.4.4. https://doi.org/10.1109/IEDM.2018.8614595.

(10) Cappelletti, P.; Annunziata, R.; Arnaud, F.; Disegni, F.; Maurelli, A.; Zuliani, P. Phase Change Memory for Automotive Grade Embedded NVM Applications. *J. Phys. D: Appl. Phys.* **2020**, *53* (19), 193002. https://doi.org/10.1088/1361-6463/ab71aa.

(11) Ielmini, D.; Wong, H.-S. P. In-Memory Computing with Resistive Switching Devices. *Nat Electron* **2018**, *1* (6), 333–343. https://doi.org/10.1038/s41928-018-0092-2.

(12) Islam, R.; Li, H.; Chen, P.-Y.; Wan, W.; Chen, H.-Y.; Gao, B.; Wu, H.; Yu, S.; Saraswat, K.; Philip Wong, H.-S. Device and Materials Requirements for Neuromorphic Computing. *J. Phys. D: Appl. Phys.* **2019**, *52* (11), 113001. https://doi.org/10.1088/1361-6463/aaf784.

(13) Sabina, S.; Abu, S.; Damien, Q.; Bipin, R. Memristive Devices for Brain-Inspired Computing, 1st Edition - June 12, 2020. https://www.elsevier.com/books/memristive-devices-for-brain-inspired-computing/spiga/978-0-08-102782-0 (accessed 2021 -05 -24).

(14) Zuliani, P.; Varesi, E.; Palumbo, E.; Borghi, M.; Tortorelli, I.; Erbetta, D.; Libera, G. D.; Pessina, N.; Gandolfo, A.; Prelini, C.; Ravazzi, L.; Annunziata, R. Overcoming Temperature Limitations in Phase Change Memories with Optimized GexSbyTez. *IEEE Trans. Electron Devices* **2013**, *60* (12), 4020–4026. https://doi.org/10.1109/TED.2013.2285403.

(15) Kiouseloglou, A.; Navarro, G.; Sousa, V.; Persico, A.; Roule, A.; Cabrini, A.; Torelli, G.; Maitrejean, S.; Reimbold, G.; De Salvo, B.; Clermidy, F.; Perniola, L. A Novel Programming Technique to Boost Low-Resistance State Performance in Ge-Rich GST Phase Change Memory.

IEEE Trans. Electron Devices **2014**, *61* (5), 1246–1254. https://doi.org/10.1109/TED.2014.2310497.

(16) Palumbo, E.; Zuliani, P.; Borghi, M.; Annunziata, R. Forming Operation in Ge-Rich GexSbyTez Phase Change Memories. *Solid-State Electronics* **2017**, *133*, 38–44. https://doi.org/10.1016/j.sse.2017.03.016.

(17) Lee, Y.-H.; Liao, P. J.; Hou, V.; Heh, D.; Nien, C.-H.; Kuo, W.-H.; Chen, G. T.; Yu, S.-M.; Chen, Y.-S.; Wu, J.-Y.; Bao, X.; Diaz, C. H. Composition Segregation of Ge-Rich GST and Its Effect on Reliability. In *2021 IEEE International Reliability Physics Symposium (IRPS)*; IEEE: Monterey, CA, USA, 2021; pp 1–6. https://doi.org/10.1109/IRPS46558.2021.9405168.

(18) Redaelli, A.; Petroni, E.; Annunziata, R. Material and Process Engineering Challenges in Ge-Rich GST for Embedded PCM. *Materials Science in Semiconductor Processing* **2022**, *137*, 106184. https://doi.org/10.1016/j.mssp.2021.106184.

(19) Cheng, H. Y.; Wu, J. Y.; Cheek, R.; Raoux, S.; BrightSky, M.; Garbin, D.; Kim, S.; Hsu, T. H.; Zhu, Y.; Lai, E. K.; Joseph, E.; Schrott, A.; Lai, S. C.; Ray, A.; Lung, H. L.; Lam, C. A Thermally Robust Phase Change Memory by Engineering the Ge/N Concentration in (Ge, N)XSbyTez Phase Change Material. In *2012 International Electron Devices Meeting*; IEEE: San Francisco, CA, USA, 2012; p 31.1.1-31.1.4. https://doi.org/10.1109/IEDM.2012.6479141.

(20) Cheng, H. Y.; Hsu, T. H.; Raoux, S.; Wu, J. Y.; Du, P. Y.; Breitwisch, M.; Zhu, Y.; Lai, E. K.; Joseph, E.; Mittal, S.; Cheek, R.; Schrott, A.; Lai, S. C.; Lung, H. L.; Lam, C. A High Performance Phase Change Memory with Fast Switching Speed and High Temperature Retention by Engineering the GexSbyTez Phase Change Material. In *2011 International Electron Devices Meeting*; IEEE: Washington, DC, USA, 2011; p 3.4.1-3.4.4. https://doi.org/10.1109/IEDM.2011.6131481.

(21) Abou El Kheir, O.; Dragoni, D.; Bernasconi, M. Density Functional Simulations of Decomposition Pathways of Ge-Rich GeSbTe Alloys for Phase Change Memories. *Phys. Rev. Materials* **2021**, *5* (9), 095004. https://doi.org/10.1103/PhysRevMaterials.5.095004.

(22) Abou El Kheir, O.; Bernasconi, M. High-Throughput Calculations on the Decomposition Reactions of Off-Stoichiometry GeSbTe Alloys for Embedded Memories. *Nanomaterials* **2021**, *11* (9), 2382. https://doi.org/10.3390/nano11092382.

(23) Cecchi, S.; Lopez Garcia, I.; Mio, A. M.; Zallo, E.; Abou El Kheir, O.; Calarco, R.; Bernasconi, M.; Nicotra, G.; Privitera, S. M. S. Crystallization and Electrical Properties of Ge-Rich GeSbTe Alloys. *Nanomaterials* **2022**, *12* (4), 631. https://doi.org/10.3390/nano12040631.

(24) Privitera, S. M. S.; López García, I.; Bongiorno, C.; Sousa, V.; Cyrille, M. C.; Navarro, G.; Sabbione, C.; Carria, E.; Rimini, E. Crystallization Properties of Melt-Quenched Ge-Rich GeSbTe Thin Films for Phase Change Memory Applications. *Journal of Applied Physics* **2020**, *128* (15), 155105. https://doi.org/10.1063/5.0023696.

(25) Agati, M.; Vallet, M.; Joulié, S.; Benoit, D.; Claverie, A. Chemical Phase Segregation during the Crystallization of Ge-Rich GeSbTe Alloys. *J. Mater. Chem. C* **2019**, *7* (28), 8720–8729. https://doi.org/10.1039/C9TC02302J.

(26) Navarro, G.; Coue, M.; Kiouseloglou, A.; Noe, P.; Fillot, F.; Delaye, V.; Persico, A.; Roule, A.; Bernard, M.; Sabbione, C.; Blachier, D.; Sousa, V.; Perniola, L.; Maitrejean, S.; Cabrini, A.; Torelli, G.; Zuliani, P.; Annunziata, R.; Palumbo, E.; Borghi, M.; Reimbold, G.; De Salvo, B. Trade-off between SET and Data Retention Performance Thanks to Innovative Materials for Phase-Change Memory. In *2013 IEEE International Electron Devices Meeting*; IEEE: Washington, DC, USA, 2013; p 21.5.1-21.5.4. https://doi.org/10.1109/IEDM.2013.6724678.

(27) Luong, M. A.; Agati, M.; Ratel Ramond, N.; Grisolia, J.; Le Friec, Y.; Benoit, D.; Claverie, A. On Some Unique Specificities of Ge-Rich GeSbTe Phase-Change Material Alloys for Nonvolatile Embedded-Memory Applications. *Phys. Status Solidi RRL* **2021**, *15* (3), 2000471. https://doi.org/10.1002/pssr.202000471.

(28) Prazakova, L.; Nolot, E.; Martinez, E.; Fillot, F.; Rouchon, D.; Rochat, N.; Bernard, M.; Sabbione, C.; Morel, D.; Bernier, N.; Grenier, A.; Papon, A.-M.; Cyrille, M.-C.; Navarro, G. Temperature Driven Structural Evolution of Ge-Rich GeSbTe Alloys and Role of N-Doping. *Journal of Applied Physics* **2020**, *128* (21), 215102. https://doi.org/10.1063/5.0027734.

(29) Desjardins, K.; Mocuta, C.; Dawiec, A.; Réguer, S.; Joly, P.; Dubuisson, J.-M.; Alves, F.; Noureddine, A.; Bompard, F.; Thiaudière, D. The CirPAD, a Circular 1.4 M Hybrid Pixel Detector Dedicated to X-Ray Diffraction Measurements at Synchrotron SOLEIL. *J Synchrotron Rad* **2022**, *29* (1), 180–193. https://doi.org/10.1107/S1600577521012492.

(30) Luong, M.; Cherkashin, N.; Pecassou, B.; Sabbione, C.; Mazen, F.; Claverie, A. Effect of Nitrogen Doping on the Crystallization Kinetics of Ge2Sb2Te5. *Nanomaterials* **2021**, *11* (7), 1729. https://doi.org/10.3390/nano11071729.

(31) Kooi, B. J.; Groot, W. M. G.; De Hosson, J. Th. M. *In Situ* Transmission Electron Microscopy Study of the Crystallization of Ge2Sb2Te5. *Journal of Applied Physics* **2004**, *95* (3), 924–932. https://doi.org/10.1063/1.1636259.

(32) Germain, P.; Zellama, K.; Squelard, S.; Bourgoin, J. C.; Gheorghiu, A. Crystallization in Amorphous Germanium. *Journal of Applied Physics* **1979**, *50* (11), 6986–6994. https://doi.org/10.1063/1.325855.

(33) Claverie, A.; Koffel, S.; Cherkashin, N.; Benassayag, G.; Scheiblin, P. Amorphization, Recrystallization and End of Range Defects in Germanium. *Thin Solid Films* **2010**, *518* (9), 2307–2313. https://doi.org/10.1016/j.tsf.2009.09.162.

(34) Shimada, Masahiko.; Dachille, Frank. Crystallization of Amorphous Germanium Telluride under Pressure. *Inorg. Chem.* **1976**, *15* (7), 1729–1730. https://doi.org/10.1021/ic50161a056.

(35) Kresse, G.; Furthmüller, J. Efficient Iterative Schemes for *Ab Initio* Total-Energy Calculations Using a Plane-Wave Basis Set. *Phys. Rev. B* **1996**, *54* (16), 11169–11186. https://doi.org/10.1103/PhysRevB.54.11169.

(36) Perdew, J. P.; Burke, K.; Ernzerhof, M. Generalized Gradient Approximation Made Simple [Phys. Rev. Lett. 77, 3865 (1996)]. *Phys. Rev. Lett.* **1997**, *78* (7), 1396–1396. https://doi.org/10.1103/PhysRevLett.78.1396.

(37) Ronneberger, I.; Zanolli, Z.; Wuttig, M.; Mazzarello, R. Changes of Structure and Bonding with Thickness in Chalcogenide Thin Films. *Adv. Mater.* **2020**, *32* (29), 2001033. https://doi.org/10.1002/adma.202001033.

(38) Okamoto, H. Ge-Sb (Germanium-Antimony). *J. Phase Equilib. Diffus.* **2012**, *33* (2), 162–162. https://doi.org/10.1007/s11669-012-9995-1.

(39) Bordas, S.; Clavaguer-Mora, M. T.; Legendre, B.; Hancheng, C. Phase Diagram of the Ternary System Ge-Sb-Te. *Thermochimica Acta* **1986**, *107*, 239–265. https://doi.org/10.1016/0040-6031(86)85051-1.

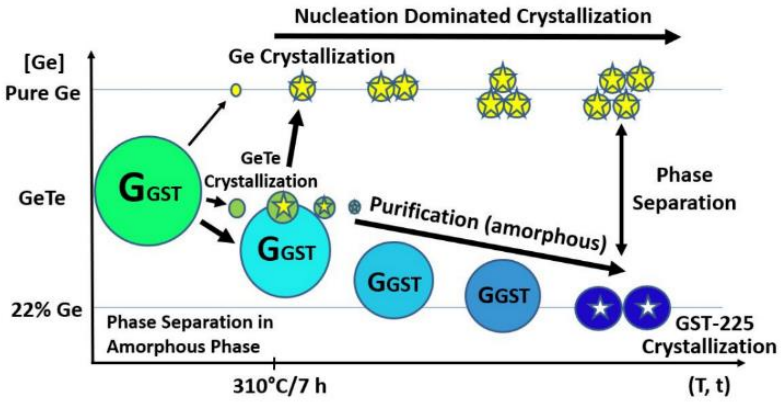
Nucleation Dominated Crystallization
[Ge]
Pure Ge
Ge Crystallization
GeTe
Crystallization
GeTe
GGST
GGST
GGST
GGST
Purification (amorphous)
Phase
Separation
22% Ge
Phase Separation in
Amorphous Phase
GST-225
Crystallization
310°C/7 h
(T, t)